

Performance of a Superconducting Quantum Battery

Samira Elghaayda ¹, Asad Ali ^{2,*}, Saif Al-Kuwari ², Artur Czerwinski ³, Mostafa Mansour ¹ and Saeed Haddadi ^{4,5,†}

¹Laboratory of High Energy Physics and Condensed Matter, Department of Physics, Faculty of Sciences of Ain Chock, Hassan II University, P.O. Box 5366 Maarif, Casablanca 20100, Morocco.

²Qatar Centre for Quantum Computing, College of Science and Engineering, Hamad Bin Khalifa University, Doha, Qatar

³Institute of Physics, Faculty of Physics, Astronomy and Informatics, Nicolaus Copernicus University in Torun, ul. Grudziadzka 5, 87-100 Torun, Poland

⁴Faculty of Physics, Semnan University, P.O. Box 35195-363, Semnan, Iran

⁵Saeed's Quantum Information Group, P.O. Box 19395-0560, Tehran, Iran

(Dated: December 2, 2024)

Finding a quantum battery model that demonstrates a quantum advantage while remaining feasible for experimental production is a considerable challenge. In this paper, we introduce a superconducting quantum battery (SQB) model that exhibits such an advantage. The model consists of two coupled superconducting qubits that interact during the unitary charging process while remaining in equilibrium with a thermal reservoir. We first describe the model, provide evidence of the quantum advantage, and then discuss the fabrication process of the battery using superconducting qubits. Importantly, we derive analytical expressions for the ergotropy, instantaneous power, and capacity of the SQB, as well as their connection to quantum coherence. We demonstrate that leveraging the collective effects of Josephson energies and the coupling energy between qubits allows for optimization, resulting in improved energy redistribution and a significant enhancement in charging efficiency. This work highlights the complexities of tuning system parameters, which increase the potential for work extraction from the quantum battery, thereby providing a deeper understanding of the charging mechanisms involved. These findings can be applied to superconducting quantum circuit battery architectures, underscoring the feasibility of efficient energy storage in these systems. Our results pave the way for proposals of new superconducting devices capable of storing extractable work, emphasizing their potential for efficient energy storage.

Keywords: superconducting qubits, Josephson energy, quantum coherence, work extraction, energy storage.

I. INTRODUCTION

Over the last twenty years, we have witnessed significant progress in quantum technologies, ranging from fundamental physics to commercial applications. This advancement has led to important developments in energy transfer mechanisms within the quantum realm and the role of quantum resources in microscopic devices [1–5]. By focusing on these advancements, one can see various physical implementations emerging as leading technologies, such as quantum batteries [6–9] and superconducting circuits [10–12]. While it is still too early to determine which of these will form the foundation of tomorrow's quantum batteries [6–9], superconducting qubits are arguably at the forefront [13]. Research in this area has progressed beyond academia and is now attracting significant interest from major technology companies, including IBM, underscoring its impact on the field.

Quantum batteries can serve as stationary systems that store energy in their excited states for later use, or as dynamic mediums that transfer energy to other systems. Traditional energy storage solutions, such as chemical batteries, face several challenges, such as slow

charging, short lifespans, and harmful environmental impacts [14]. Despite some fundamental limitations [15], quantum batteries are designed to tackle these challenges by leveraging superabsorption and superradiant states, which allow multiple quantum systems to absorb energy more efficiently than classical systems, allowing faster charging rates with minimal energy loss during charging and discharging [16, 17]. Progress has been made in developing these tiny devices experimentally [18].

Superconducting qubits made from Josephson junctions are promising for quantum sensing, hybrid systems, and large-scale quantum computing architectures [10–12]. Current qubits operate below 10 GHz using standard cryogenic microwave equipment. Higher frequencies broaden the range of energies available for quantum experiments, enabling connections to a wider array of signals and quantum emitters, and allowing for higher operating temperatures. This scalability method leverages enhanced cooling power with even a slight increase in temperature [19]. Thermally robust qubits could reduce hardware demands for microwave quantum interconnects [20, 21], integrate with superconducting digital logic [22], and help manage heat from growing numbers of qubit control lines [23] as superconducting quantum processors scale to hundreds of qubits [24]. Resilient qubits in hybrid quantum systems could simplify experiments and improve performance [10, 11].

* asal68826@hbku.edu.qa

† haddadi@semnan.ac.ir

Optimizing charging processes is a core objective in quantum battery research. Effective quantum control techniques are essential for enabling faster and more reliable charging. Recently, many researchers studying the charging of quantum batteries have shown that quantum coherence and entanglement significantly enhance charging speed and energy storage efficiency [25, 26]. Furthermore, research on the scalability of quantum battery performance with system size reveals that collective quantum effects enable enhanced energy extraction beyond classical capabilities [27–33]. However, the charging protocols often rely on specific initial battery states. This dependence on the state of the quantum battery remains relatively unexplored. In this work, along these lines, we address and highlight a superconducting quantum battery (SQB) initialized in a thermal state. This battery is constructed from superconducting charge qubits with symmetric Josephson junction energies. These qubits are capacitively coupled and shunted with a large capacitance to suppress charge noise. Known as Transmon qubits, these devices function as artificial atoms, allowing us to harness their Josephson energies—particularly the mutual coupling energy between qubits—to drive ergotropy production. Experimentally, SQBs represent a cutting-edge paradigm in quantum energy storage [13], aiming to exploit quantum correlations and superposition to achieve charging capabilities that surpass those of conventional electrochemical batteries in efficiency and performance.

A. Contribution and Motivation

The quest for efficient quantum battery models that exhibit quantum advantages is a pressing challenge in advancing quantum technology. Superconducting qubits, with their established role in quantum computing, offer a promising platform for realizing such quantum batteries. However, developing a feasible design that is both experimentally implementable and optimizes energy transfer requires careful consideration of coherence and interaction dynamics within the system. In this work, we propose a SQB model based on two coupled superconducting qubits. This model demonstrates a significant quantum advantage in energy storage and extraction while remaining achievable for experimental realization. By analyzing the SQB’s ergotropy, power, and capacity, we identify key factors—such as coherence and qubit coupling—that maximize work extraction, illustrating how collective effects from Josephson energies and inter-qubit coupling enhance charging efficiency. This SQB model connects the quantum properties of the system with practical considerations for device fabrication, laying a foundation for developing high-performance energy storage in superconducting quantum circuits.

B. Organization

In this work, we focus on the role of coherence in ergotropic work extraction. We begin by briefly reviewing the relevant model of two superconducting charge qubits (SCQs) in Sec. II. The remainder of this section discusses the fabrication of the SQB within this framework and presents the details of the charging process. It also includes fundamental performance indicators for SQBs, such as ergotropy, power, capacity, and coherence. In Sec. III, we qualitatively describe the results and insights gained regarding the performance of the SQB. We summarize our findings and discuss potential future research directions in the final section, Sec. IV.

II. MODEL AND PERFORMANCE OF SQB

The current model consists of two single Cooper-pair box charge qubits coupled through a fixed capacitor [34–37]. Superconducting materials in the model exhibit a suppressed transition temperature T_c , which is carefully adjusted by selecting suitable materials, typically achieving values in the milli-Kelvin temperature range to facilitate efficient and scalable superconducting circuits. A representative example is a superconducting trilayer made of Al/Ti/Au, with respective layer thicknesses of 300 Å, 200 Å, and 200 Å, and a transition temperature of $T_c = 450$ mK [34–37]. The Hamiltonian of a two-superconducting-qubit system can be expressed by [34]

$$\begin{aligned} \mathcal{H} = & -\frac{1}{2} \left\{ \left[4\xi_{c1} \left(\frac{1}{2} - n_{g1} \right) + 2\xi_c \left(\frac{1}{2} - n_{g2} \right) \right] \sigma_{z1} \right. \\ & + \left[4\xi_{c2} \left(\frac{1}{2} - n_{g2} \right) + 2\xi_c \left(\frac{1}{2} - n_{g1} \right) \right] \sigma_{z2} \\ & \left. + \xi_1 \sigma_{x1} + \xi_2 \sigma_{x2} - 2\xi_c \sigma_{zz} \right\}, \end{aligned} \quad (1)$$

where:

- ξ_{c1} and ξ_{c2} are the charging energies.
- ξ_1 and ξ_2 are the Josephson energies.
- ξ_c is the mutual coupling energy between the two qubits.
- $\sigma_{x1} = \sigma_x \otimes I$, $\sigma_{x2} = I \otimes \sigma_x$, and $\sigma_{zz} = \sigma_z \otimes \sigma_z$, with $\sigma_{x,z}$ being Pauli matrices and I is the identity matrix.
- $n_{gj} = \frac{C_{gj}V_{gj}}{2e}$ is the normalized qubit gate charge, where C_{gj} and V_{gj} are the control gate capacitance and voltage, respectively.

For simplicity, calculations are restricted to the degeneracy point, where $n_{g1} = n_{g2} = 0.5$, a condition that ensures insensitivity to noise [35]. Under this condition, the model Hamiltonian simplifies to

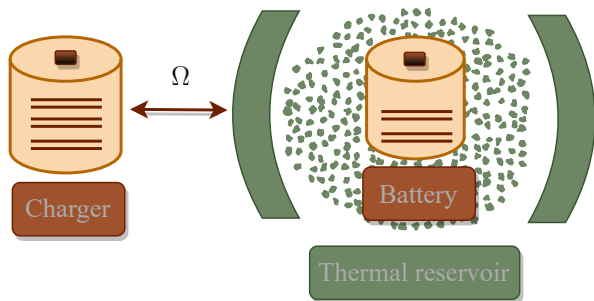


FIG. 1. Schematic diagram of the charging process of the quantum battery.

$$\mathcal{H}_B = -\frac{1}{2} [\xi_1 \sigma_{x1} + \xi_2 \sigma_{x2} - \xi_c \sigma_{zz}]. \quad (2)$$

The above Hamiltonian in matrix form yields

$$\mathcal{H}_B = \frac{1}{2} \begin{pmatrix} 2\xi_c & -\xi_2 & -\xi_1 & 0 \\ -\xi_2 & -2\xi_c & 0 & -\xi_1 \\ -\xi_1 & 0 & -2\xi_c & -\xi_2 \\ 0 & -\xi_1 & -\xi_2 & 2\xi_c \end{pmatrix}. \quad (3)$$

At $t = 0$, if the system is fully discharged, its initial state can be the ground state $\mathcal{R}(0) = |00\rangle\langle 00|$ at absolute zero or Gibbs state at any finite temperature. The effectiveness of a quantum battery depends on a robust charging process; however, these processes are often sensitive to the initial state of the battery. We assume the Gibbs state as the initial state of QB instead of ground state as it is practical experimentally to deal with finite temperature QB than QB at ground state. Therefore, for a system at finite temperature T , we introduce the initial state described by the Gibbs thermal state:

$$\mathcal{R}_{th}(0) = \frac{e^{-\beta\mathcal{H}_B}}{\mathcal{Z}}, \quad (4)$$

where $\beta = \frac{1}{k_B T}$ is the inverse temperature (set the Boltzmann constant $k_B = 1$) and $\mathcal{Z} = \text{Tr}(e^{-\beta\mathcal{H}_B})$ is the partition function. This thermal state represents the probability distribution of the energy eigenstates of the system at the specified temperature. Given the structure of the Hamiltonian, the thermal state can be expressed as follows:

$$\mathcal{R}_{th}(0) = \frac{1}{\mathcal{Z}} \begin{pmatrix} \mathcal{R}_{th11} & \mathcal{R}_{th12} & \mathcal{R}_{th13} & \mathcal{R}_{th14} \\ \mathcal{R}_{th21} & \mathcal{R}_{th22} & \mathcal{R}_{th23} & \mathcal{R}_{th24} \\ \mathcal{R}_{th31} & \mathcal{R}_{th32} & \mathcal{R}_{th33} & \mathcal{R}_{th34} \\ \mathcal{R}_{th41} & \mathcal{R}_{th42} & \mathcal{R}_{th43} & \mathcal{R}_{th44} \end{pmatrix}. \quad (5)$$

The above matrix elements are reported in Appendix A.

Now, we can evaluate the performance of our SQB by charging it via the Pauli-X gate-based charging Hamiltonian, which is discussed in the following subsections. The

model consists of two coupled superconducting qubits that interact during the unitary charging process while remaining in equilibrium with a thermal reservoir (see Fig. 1).

A. Charging closed SQB with Pauli-X gate

Let us consider a closed SQB, where charging protocols are necessarily unitary. First, we note that for almost density matrix, there exists a unitary map that increases its energy. This can be understood by recognizing that the problem of charging with respect to \mathcal{H}_B is equivalent to discharging with respect to $-\mathcal{H}_B$. Therefore, the only states that cannot be charged using a unitary protocol are those whose ergotropy [38] with respect to $-\mathcal{H}_B$ is zero. From Refs. [39–41], we conclude that the only states that cannot be charged by any unitary operation are those that are diagonal in the eigenbasis of \mathcal{H}_B with eigenvalues that are non-decreasing in energy.

The SQB can be charged by applying a local field pulse in the x -direction with pulse strength $\Omega = \Omega(t)$. The expression for the charging Hamiltonian (\mathcal{H}_{c_x}) in x -direction is

$$\mathcal{H}_{c_x} = \Omega(\sigma_x \otimes \mathbb{I}_2 + \mathbb{I}_2 \otimes \sigma_x). \quad (6)$$

In practice, the operation of the X-gate in superconducting qubits is achieved by applying a microwave pulse that induces a transition between the qubit's ground state $|0\rangle$ and excited state $|1\rangle$. This pulse, resonant with the qubit's transition frequency, is shaped to effect a π -radian rotation around the x -axis of the Bloch sphere, thus flipping the qubit's state. The pulse duration, amplitude, and phase are calibrated to ensure high-fidelity state inversion. Typically, a quantum battery is charged by delivering uniform pulses to all quantum cells. During the charging process, once the quantum battery reaches its peak value, $t \rightarrow \tau$, the x -direction pulse is turned off to prevent the quantum battery from returning to its initial state. In a closed system, the charging process can be implemented using the unitary operation

$$\mathcal{U}_X(t) = \exp[-i\mathcal{H}_{c_x}t], \quad (7)$$

which drives the qubit system from its initial state. The unitary operator for X-gate charging can be explicitly expressed as

$$\mathcal{U}_X(t) = \begin{pmatrix} a & c & c & b \\ c & a & b & c \\ c & b & a & c \\ b & c & c & a \end{pmatrix}, \quad (8)$$

here, $a = \cos^2(\tau)$, $b = -\sin^2(\tau)$, and $c = -i \sin(\tau) \cos(\tau)$ with $\tau = \Omega t$.

B. Ergotropy, power, capacity, and quantum coherence

To gain more insights into the working of our system, we analyze our Hamiltonian through spectral decomposition given by

$$\mathcal{H}_B = \sum_{i=1}^4 \epsilon_i |\Delta_i\rangle\langle\Delta_i|, \text{ with } \epsilon_{i+1} \geq \epsilon_i. \quad (9)$$

In this context, ϵ_i 's represent the eigenvalues, and $|\Delta_i\rangle$'s denote the corresponding eigenstates. This representation is helpful for assessing energy changes and work extraction potential in cyclic unitary processes, which suggests that the Hamiltonian of the quantum battery must be the same at the end as it was in its initial state.

The state \mathcal{R} is expressed as:

$$\mathcal{R} = \sum_{j=1}^4 \lambda_j |e_j\rangle\langle e_j|, \text{ where } \lambda_{j+1} \leq \lambda_j. \quad (10)$$

The goal is to convert the system from the state \mathcal{R} to a state with lower internal energy to extract the energy difference. After extracting the maximum amount of work in a cyclic and unitary process, the system reaches a passive state π [38, 40, 42, 43]. This passive state is diagonal in the Hamiltonian's eigenbasis and has a decreasing population with increasing energy levels. We define this passive state as $\pi = \mathcal{R}_{th}$, a Gibbs thermal state. To gain a deeper understanding of energy extraction efficiency from quantum states, it is important to study the maximum amount of work that can be extracted from a quantum system through a cyclic unitary process, a concept known as ergotropy. This process involves transitioning the system from its initial state to a thermal state. Ergotropy is defined as:

$$\mathcal{E} := \sum_{m,n} \lambda_m \epsilon_n [|\langle\Delta_n|e_m\rangle|^2 - \delta_{mn}], \quad (11)$$

where δ_{mn} is the Kronecker delta. Alternatively,

$$\mathcal{E} := \text{Tr}[(\mathcal{R} - \mathcal{R}_{th})\mathcal{H}_B]. \quad (12)$$

The figure of merit we use to analyze this model is ergotropy and average power of SQB. Note that the instantaneous power of a quantum battery is defined as $\mathcal{P} = d\mathcal{E}/dt$.

If the final state is another non-passive state Π , the work done is:

$$\mathcal{W} = \text{Tr}[(\mathcal{R} - \Pi)\mathcal{H}_B]. \quad (13)$$

Furthermore, the capacity of a quantum battery, denoted as \mathcal{K} , serves as an effective performance indicator [44]. This metric allows us to gain meaningful insights

into the quantum battery without the need to solve intricate dynamical equations. The capacity of a quantum battery is characterized as:

$$\mathcal{K} = \text{Tr}[\mathcal{H}_B \hat{\rho}_\uparrow] - \text{Tr}[\mathcal{H}_B \hat{\rho}_\downarrow], \quad (14)$$

where $\hat{\rho}_\downarrow = |0^{\otimes N}\rangle\langle 0^{\otimes N}|$ and $\hat{\rho}_\uparrow = |1^{\otimes N}\rangle\langle 1^{\otimes N}|$ represent the ground and excited states of the N -partite quantum battery, respectively. For our specific case of two qubits, $N = 2$. This measure directly quantifies the energy gap between the quantum battery's maximum and minimum energy states. Its calculation is straightforward and does not involve time-dependent optimization, making it suitable for both open and closed quantum batteries. As such, \mathcal{K} provides a practical and efficient metric for evaluating quantum battery performance.

In order to keep track of the degree of the quantum coherence existing inside SQB while the work is being extracted in the form of ergotropy, we evaluate l_1 -norm of quantum coherence [45]. Specifically, we consider the following density matrix

$$\mathcal{R}_X(t) = \mathcal{U}_X(t)\mathcal{R}_{th}(0)\mathcal{U}_X(t)^\dagger, \quad (15)$$

where $\mathcal{R}_{th}(0)$ and $\mathcal{U}_X(t)$ are defined in Eqs. (5) and (8), respectively. The explicit form of the $\mathcal{R}_X(t)$ is given in the Appendix B. Hence, one can evaluate the l_1 -norm of quantum coherence as follows

$$\mathcal{C}_{l_1}(\mathcal{R}_X(t)) = \sum_{i \neq j} |\langle i|\mathcal{R}_X(t)|j\rangle|. \quad (16)$$

Note that we provide the closed-form expressions for the performance metrics in Appendix C.

III. RESULTS AND DISCUSSION

In Fig. 2, we present the variations of key quantities associated with our model: ergotropy \mathcal{E} , instantaneous power \mathcal{P} , capacity \mathcal{K} , and the l_1 -norm of coherence \mathcal{C}_{l_1} as functions of $\tau = \Omega t$ for different values of ξ_2 . The other parameters are fixed with $\xi_1 = 1.5$, $T = 0.5$, and $\xi_c = 0.05$.

Figure 2(a) depicts the plots of ergotropy, \mathcal{E} , as a function of τ . Ergotropy, representing the extractable work from the quantum system, displays oscillatory behavior, signifying energy fluctuations within the system's quantum state. The amplitude of these oscillations increases with ξ_2 , the Josephson energy of the second qubit. This suggests that larger values of ξ_2 enhance the system's ability to store and extract work, making it more efficient for quantum energy storage or harvesting applications. These results imply that tuning the Josephson energy of the second qubit could optimize the quantum battery's performance in terms of maximizing its stored work.

Figure 2(b) illustrates the instantaneous power, \mathcal{P} , which reflects the rate at which energy is either being extracted from or injected into the system. Positive values

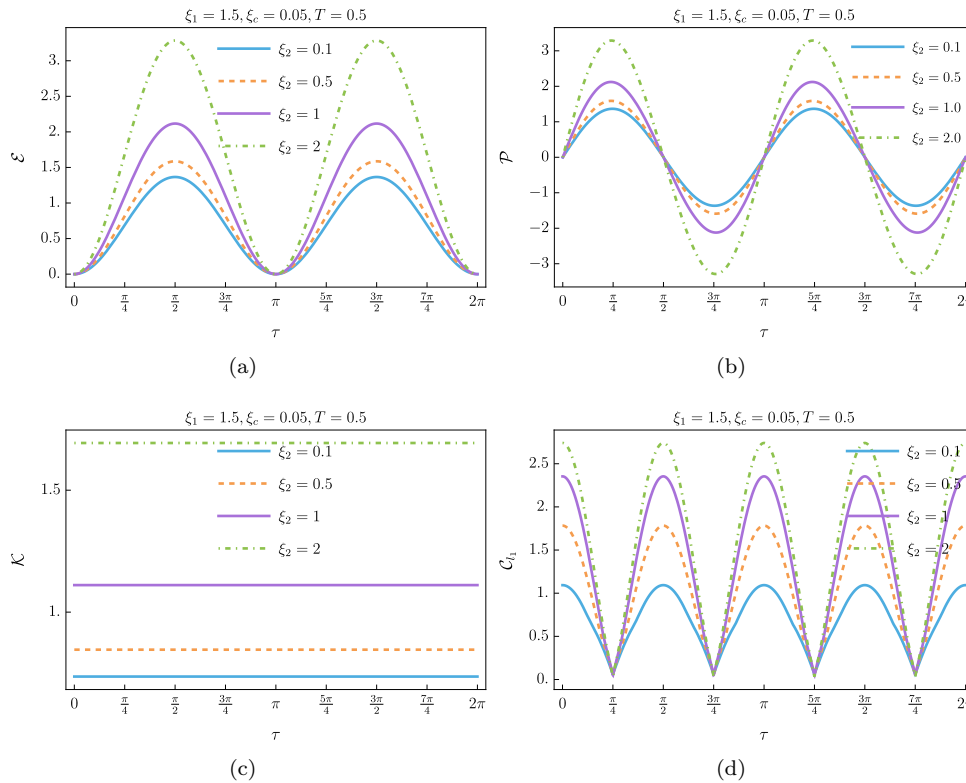


FIG. 2. Variation of (a) ergotropy \mathcal{E} , (b) instantaneous power \mathcal{P} , (c) capacity \mathcal{K} , and (d) l_1 -norm of coherence \mathcal{C}_{l_1} as a function of $\tau = \Omega t$ for different values of ξ_2 . For all plots, the fixed parameters are $\xi_1 = 1.5$, $\xi_c = 0.05$, and $T = 0.5$.

of \mathcal{P} correspond to charging the quantum battery, while negative values indicate discharging. The oscillatory nature of \mathcal{P} corresponds to the behavior of ergotropy in Fig. 2(a). For instance, during the interval $\tau \in (0; \pi/2)$, $\mathcal{P} > 0$, meaning the system is charging the quantum battery. This aligns with the increasing ergotropy over the same interval, which achieves the maximum value for $\tau = \pi/2$. Conversely, for $\tau \in (\pi/2; \pi)$, \mathcal{P} becomes negative, indicating that the system is discharging, as reflected by the decreasing ergotropy. At $\tau = \pi$, ergotropy drops to zero, marking the point where the system has fully discharged, and the sign of \mathcal{P} flips, indicating the start of a new charging cycle. This periodic behavior of charging and discharging continues, governed by the system's oscillatory dynamics.

The dependence of power, \mathcal{P} , on ξ_2 is significant; for larger values of ξ_2 , there is a noticeable increase in the peak values of oscillation. This behavior demonstrates the impact of system parameters on the dynamic performance of energy extraction processes.

Figure 2(c) displays the capacity \mathcal{K} as a function of τ . In contrast to the other quantities, the capacity remains a constant function in the domain of τ . However, the constant value of \mathcal{K} increases with larger ξ_2 , indicating that an enhanced inductive energy allows for greater information transmission capabilities in the system. This behavior suggests a stable performance in terms of ca-

capacity, which is advantageous for maintaining effective communication in quantum protocols, regardless of the oscillatory behaviors observed in ergotropy and power.

Figure 2(d) examines the l_1 -norm of coherence \mathcal{C}_{l_1} . The coherence exhibits a more complex behavior, with clear periodic features reflecting the underlying quantum interference effects. As ξ_2 increases, the coherence shows enhanced oscillatory behavior, suggesting that increased coupling may facilitate better preservation of quantum coherence in the system. This coherence is essential for maximizing the performance of quantum protocols, further illustrating the importance of parameter selection in the optimization of quantum resources.

Overall, Fig. 2 shows the interplay between ergotropy, instantaneous power, capacity, and coherence. The results indicate that careful tuning of the parameters, particularly ξ_2 , can significantly influence the efficiency of energy extraction and the preservation of quantum coherence, which are critical for the development of advanced quantum technologies.

In Fig. 3, we present the variations of ergotropy \mathcal{E} , instantaneous power \mathcal{P} , capacity \mathcal{K} , and the l_1 -norm of coherence \mathcal{C}_{l_1} as functions of $\tau = \Omega t$ for varying values of ξ_1 . The other parameters are fixed with $\xi_2 = 1.5$, $\xi_c = 0.5$, and $T = 0.1$.

Figure 3(a) presents the ergotropy \mathcal{E} as a function of τ . While the general oscillatory behavior is similar to

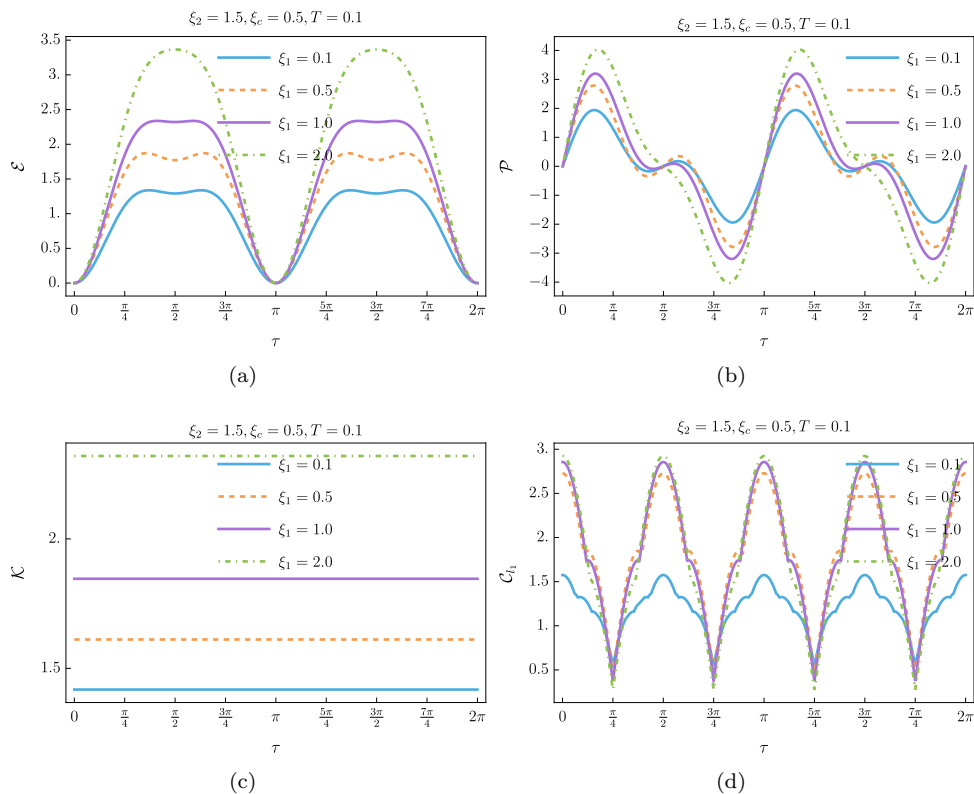


FIG. 3. Variation of (a) ergotropy \mathcal{E} , (b) instantaneous power \mathcal{P} , (c) capacity \mathcal{K} , and (d) l_1 -norm of coherence \mathcal{C}_{l_1} as a function of $\tau = \Omega t$ for different values of ξ_1 . For all plots, the fixed parameters are $\xi_2 = 1.5$, $\xi_c = 0.5$, and $T = 0.1$.

that observed in Fig. 2(a), the patterns differ due to the distinct roles played by ξ_1 and ξ_2 . In Fig. 3(a), ξ_1 , the Josephson energy of the first qubit, is varied while ξ_2 is held fixed. As ξ_1 increases, the amplitude of ergotropy oscillations grows, indicating an enhancement in the SQB's work extraction potential. This result emphasizes the significance of ξ_1 in determining the system's energy dynamics, as it directly governs the properties of the first qubit. However, the influence of ξ_1 is modulated by the coupling energy ξ_c , which governs the interaction strength between the two qubits. The higher value of ξ_c in case of Fig. 3(a) ($\xi_c = 0.5$) leads to more diverse shapes, reflecting the stronger interplay between the qubits. In contrast, Fig. 2(a) displayed smoother oscillations due to a weaker coupling $\xi_c = 0.05$.

Figure 3(b) illustrates the instantaneous power \mathcal{P} as a function of τ , showing a similar oscillatory behavior as in Fig. 2(b), but with a notable increase in complexity. The variation of ξ_1 affects the power dynamics differently than ξ_2 due to the stronger coupling strength ξ_c . Here, the non-sinusoidal oscillations become more noticeable, indicating enhanced energy exchange between the two qubits. The peak values of instantaneous power also grow with increasing ξ_1 , reinforcing the role of this parameter in optimizing energy extraction. The higher coupling strength ξ_c amplifies the interaction between the qubits, causing their dynamics to be more interdependent and resulting

in a more complex power profile compared to Fig. 2(b).

The comparison between Figs. 2 and 3 in terms of the ergotropy and the instantaneous power highlights the interplay between the Josephson energies and the coupling strength. In Fig. 2, where ξ_c is weaker, the influence of ξ_2 dominates, leading to smoother oscillatory behaviors. In contrast, the stronger coupling in Fig. 3 redistributes the influence of ξ_1 and ξ_2 , resulting in more complex dynamics. These observations demonstrate that ξ_c plays a crucial role in shaping the energy and power dynamics of the system and it must be carefully considered in the design of efficient quantum batteries.

Figure 3(c) presents the capacity \mathcal{K} as a function of τ . As in Fig. 2(c), the capacity is a constant function in the domain of τ , yet its value increases for larger ξ_1 . This stability in capacity, despite oscillations in ergotropy and power, indicates a consistent performance in information transmission capabilities across varying parameter regimes, similar to the observations made in Fig. 2.

Figure 3(d) examines the l_1 -norm of coherence \mathcal{C}_{l_1} . The coherence showcases oscillatory behavior, paralleling the dynamics observed in Fig. 2(d). As ξ_1 increases, the oscillations become more significant, indicating that higher values of ξ_1 enhance the coherence properties of the quantum state. However, this improvement appears to plateau at higher values of ξ_1 , as the corresponding plots converge and nearly overlap, suggesting a saturation

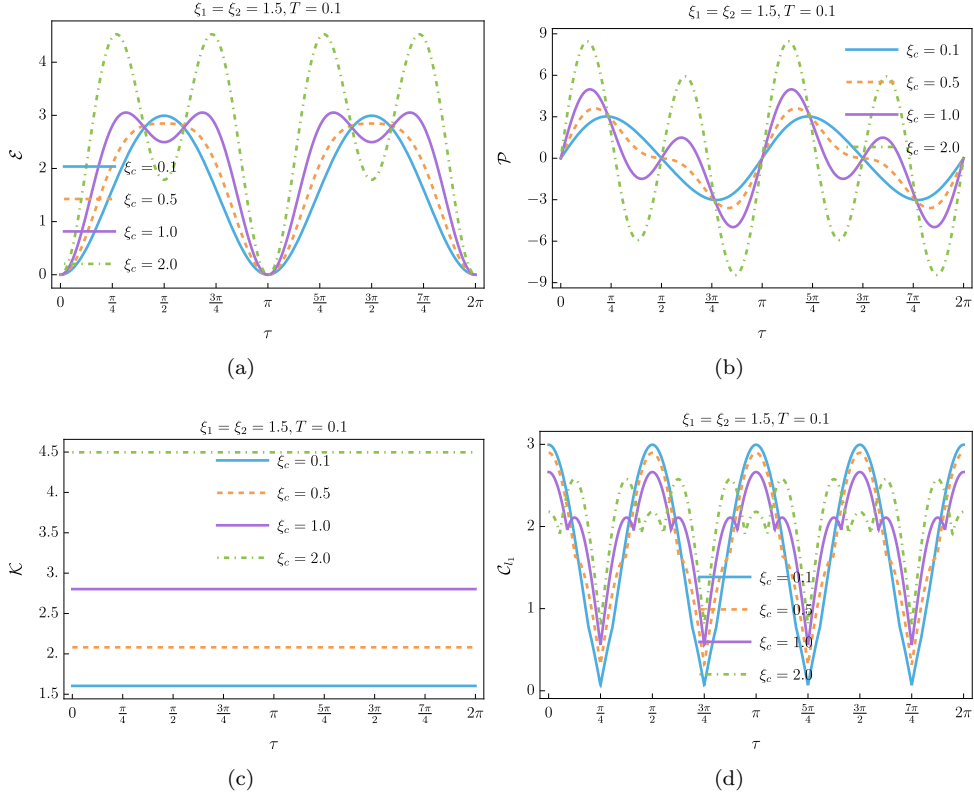


FIG. 4. Variation of (a) ergotropy \mathcal{E} , (b) instantaneous power \mathcal{P} , (c) capacity \mathcal{K} , and (d) l_1 -norm of coherence \mathcal{C}_{l_1} as a function of $\tau = \Omega t$ for different values of ξ_c . For all subfigures, $\xi_1 = \xi_2 = 1.5$ and $T = 0.1$.

tion effect where further increases in ξ_1 does not yield to coherence enhancement.

The results in Fig. 3 mirror several trends observed in Fig. 2, demonstrating the key role of parameter selection in optimizing the system's performance. The coherent interplay between ergotropy, instantaneous power, capacity, and coherence highlights the complex dynamics of energy extraction and information transmission in quantum systems.

In Fig. 4, we explore the variations of ergotropy \mathcal{E} , instantaneous power \mathcal{P} , capacity \mathcal{K} , and the l_1 -norm of coherence \mathcal{C}_{l_1} as functions of $\tau = \Omega t$ for varying values of ξ_c . The remaining parameters are fixed with $\xi_1 = \xi_2 = 1.5$ and $T = 0.1$. Fig. 4(a) depicts the plots of ergotropy \mathcal{E} with respect to τ . As observed in Figs. 2(a) and 3(a), the ergotropy exhibits oscillatory behavior. Notably, for higher values of ξ_c , not only does the amplitude of oscillation increase, but the frequency of oscillation also rises. This phenomenon indicates that larger values of the coupling energy between the qubits allow for more frequent cycles of charging and discharging within the same time interval. Physically, this can be interpreted as the system becoming more dynamic, where the energy states transition more rapidly, thereby enhancing the potential for more rapid charging of the quantum battery.

Figure 4(b) shows the instantaneous power \mathcal{P} , which continues to exhibit similar oscillatory behavior as ob-

served in Figs. 2(b) and 3(b). The increased amplitude and frequency of oscillation with larger ξ_c parallel the trends noted in ergotropy. This suggests that the power output of the system also improves, providing more energy within a given time frame. The correlation between ergotropy and instantaneous power reinforces the observation that an enhanced coupling energy directly translates into a greater efficiency of the quantum battery.

Figure 4(c) illustrates the capacity \mathcal{K} , which remains constant across the various values of τ , as in Figs. 2(c) and 3(c). However, the value of \mathcal{K} is directly influenced by ξ_c : increasing ξ_c leads to a higher constant value of capacity throughout the domain of τ . This suggests that while energy extraction fluctuates with ergotropy and power, the system's information transmission capabilities are enhanced by larger ξ_c , maintaining a stable and robust performance across the domain of τ .

Figure 4(d) examines the l_1 -norm of coherence \mathcal{C}_{l_1} . Similar to the behavior observed in Figs. 2(d) and 3(d), \mathcal{C}_{l_1} shows oscillatory behavior as ξ_c increases. However, unlike ergotropy and instantaneous power, the amplitude of the oscillations in coherence slightly declines with increasing ξ_c , despite the frequency of oscillation increasing. This decline in amplitude suggests that although the qubits become more strongly coupled, leading to more frequent state transitions (i.e., more maxima), the overall ability of the system to maintain a high level of coher-

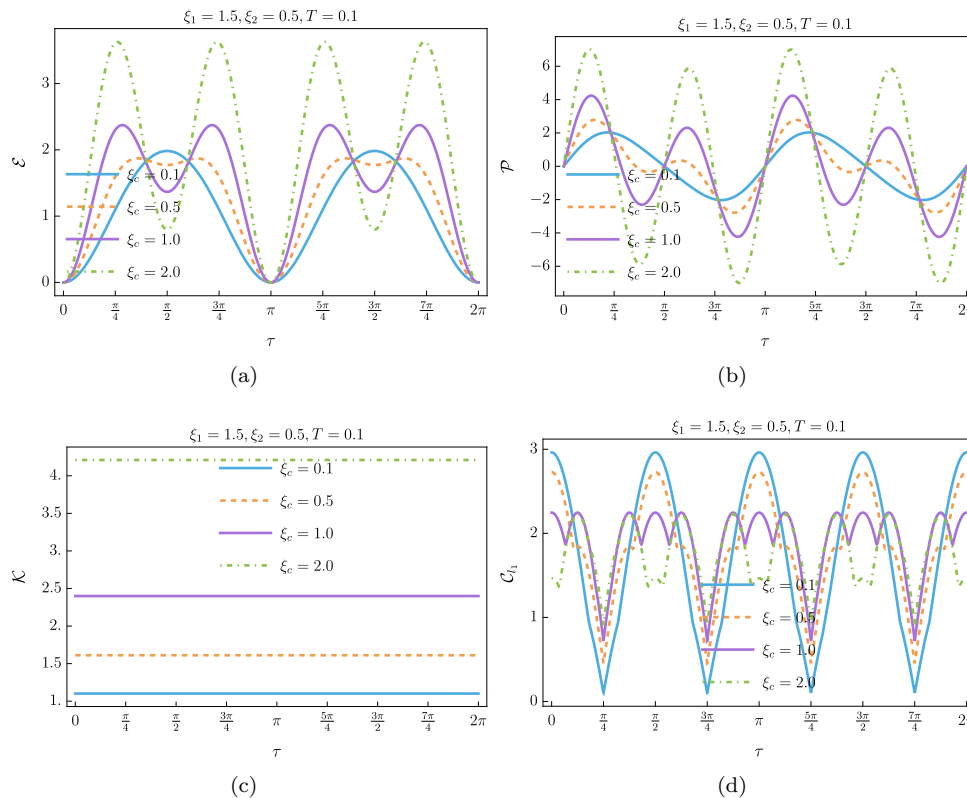


FIG. 5. Variation of (a) ergotropy \mathcal{E} , (b) instantaneous power \mathcal{P} , (c) capacity \mathcal{K} and (d) l_1 -norm of coherence \mathcal{C}_{l_1} as a function of $\tau = \Omega t$ for different values of ξ_c . For all subfigures, $\xi_1 = 1.5$, $\xi_2 = 0.5$, and $T = 0.1$.

ence diminishes slightly. Physically, this could reflect the increased interaction between the qubits causing more rapid fluctuations in coherence but limiting the maximum achievable coherence at any given time.

In general, the results presented in Fig. 4 highlight the impact of the coupling energy ξ_c between qubits on the system's energy dynamics and coherence properties. In particular, increasing ξ_c enhances the frequency of oscillations in ergotropy, instantaneous power, and coherence, indicating that the system becomes more dynamic and responsive. However, while both ergotropy and power exhibit increases in both amplitude and frequency, coherence shows an interesting trade-off: the frequency of oscillations increases, but the amplitude slightly declines. This suggests that stronger qubit coupling facilitates more rapid state transitions, but at the cost of slightly reducing the overall coherence levels. This observation showcases a delicate balance between coherence and energy extraction in strongly coupled quantum systems.

Finally, in Fig. 5, we analyze the variations of ergotropy \mathcal{E} , instantaneous power \mathcal{P} , capacity \mathcal{K} , and the l_1 -norm of coherence \mathcal{C}_{l_1} as functions of $\tau = \Omega t$ for different values of the coupling strength ξ_c . The other parameters are fixed with $\xi_1 = 1.5$, $\xi_2 = 0.5$, and $T = 0.1$.

Figure 5(a) depicts the plots of ergotropy \mathcal{E} with respect to τ . While the overall tendencies are similar to

those in Figure 4(a), we observe that the maximum values of ergotropy are significantly lower, which means that the maximum amount of energy stored in the quantum battery is reduced. This is due to the smaller value of ξ_2 , which represents the Josephson energy of the second qubit. With $\xi_1 = 1.5$ and $\xi_2 = 0.5$, the asymmetry in the Josephson energies of the qubits reduces the system's ability to extract work. The oscillatory nature persists, with both the amplitude and frequency increasing as ξ_c increases. However, the reduction in ξ_2 limits the overall ergotropy, as the second qubit contributes less energy to the system.

Figure 5(b) shows the instantaneous power \mathcal{P} . Similar to the trends observed in ergotropy, the maximum values of \mathcal{P} are lower compared to Fig. 4(b). This again reflects the reduced Josephson energy of the second qubit, which lowers the power output of the system. The oscillations in power increase in both amplitude and frequency as ξ_c increases, consistent with the behavior of ergotropy. The coupling strength ξ_c enhances the rate of energy transfer between the qubits, but the total available energy is constrained by the smaller value of ξ_2 .

Figure 5(c) illustrates the capacity \mathcal{K} , which also shows lower overall values. The reduced capacity is directly related to the reduced Josephson energy of the second qubit, $\xi_2 = 0.5$, which lowers the system's ability to store and transfer information. As in Fig. 4(c), capacity in-

creases with the quantity ξ_c , indicating that \mathcal{K} is affected by both the coupling strength and the Josephson energies of the qubits.

Figure 5(d) examines the l_1 -norm of coherence \mathcal{C}_{l_1} . The general behavior of coherence is similar to that in Fig. 4(d), with oscillations increasing in frequency as ξ_c increases. The amplitude of the oscillations in \mathcal{C}_{l_1} is also declining as we increase the values of ξ_c . Moreover, while the coupling strength enhances the frequency of coherence oscillations, the asymmetry between the qubits' Josephson energies ($\xi_1 = 1.5$ and $\xi_2 = 0.5$) reduces the maximum achievable coherence as compared with Fig. 4(d).

The results in Fig. 5 highlight the impact of the asymmetry in Josephson energies between the two qubits on the system's performance. With $\xi_1 = 1.5$ and $\xi_2 = 0.5$, the overall ergotropy, instantaneous power, and capacity are significantly reduced compared to the results in Fig. 4. This suggests that the energy imbalance between the qubits limits their collective ability to extract work, generate power, and store information, influencing the overall performance of the quantum battery. However, the coupling strength ξ_c still plays a key role in increasing the frequency of oscillations in ergotropy, power, and coherence, demonstrating that stronger coupling facilitates more dynamic interactions between the qubits.

IV. DISCUSSION AND CONCLUSIONS

In this paper, we investigated the performance of SQB charging using a quantum system composed of two superconducting coupled qubits, specifically focusing on the variation of key thermodynamic and informational quantities: ergotropy \mathcal{E} , instantaneous power \mathcal{P} , capacity \mathcal{K} , and the l_1 -norm of coherence \mathcal{C}_{l_1} . By systematically varying the coupling strength ξ_c as well as the Josephson energies of the qubits ξ_1 and ξ_2 , we have explored how these parameters influence the performance of the quantum battery.

Our analysis demonstrates several significant findings. First, we observe that for all values of the coupling strength ξ_c , the system exhibits oscillatory behavior in ergotropy, instantaneous power, and coherence. These oscillations reflect the underlying quantum energy transfer dynamics between the two qubits. As ξ_c increases, both the amplitude and frequency of these oscillations increase. This tendency means that stronger coupling enhances the energy exchange between the qubits and results in more rapid transitions within the system. However, in cases where there is an asymmetry between the Josephson energies of the qubits, particularly when ξ_2 is significantly smaller than ξ_1 , the maximum achievable ergotropy and power are limited. This implies that a balance in the Josephson energies of the qubits is crucial for maximizing the system's performance, particularly for work extraction and power generation.

In terms of information capacity \mathcal{K} , we find that this quantity varies with each value of ξ_c and is influenced by the Josephson energies of the qubits. This variation reflects the fact that the performance of the system is

closely tied to both the energy properties of the qubits and the coupling strength. Systems with higher Josephson energies exhibit greater capacity, enabling them to store more energy. However, the results also indicate that when one qubit has significantly lower Josephson energy than the other (as shown in Fig. 5), the system's overall information capacity is reduced.

Thus, to achieve optimal objective functions, a detailed analysis of SQB parameters is considered valuable.

Appendix A: Elements of thermal state

The elements of thermal state (5) are

$$\mathcal{R}_{th_{11}} = \mathcal{R}_{th_{44}} = \frac{A_- + A_+ - \frac{2B_- \xi_c}{\alpha_-} - \frac{2B_+ \xi_c}{\alpha_+}}{4(A_- + A_+)}, \quad (\text{A1})$$

$$\mathcal{R}_{th_{12}} = \mathcal{R}_{th_{21}} = \frac{\frac{B_- (\xi_2 - \xi_1)}{2\alpha_-} + \frac{B_+ (\xi_1 + \xi_2)}{2\alpha_+}}{2(A_- + A_+)}, \quad (\text{A2})$$

$$\mathcal{R}_{th_{13}} = \mathcal{R}_{th_{31}} = \frac{\frac{B_- (\xi_1 - \xi_2)}{2\alpha_-} + \frac{B_+ (\xi_1 + \xi_2)}{2\alpha_+}}{2(A_- + A_+)}, \quad (\text{A3})$$

$$\mathcal{R}_{th_{14}} = \mathcal{R}_{th_{41}} = \frac{-A_- + A_+ + \frac{2B_- \xi_c}{\alpha_-} - \frac{2B_+ \xi_c}{\alpha_+}}{4(A_- + A_+)}, \quad (\text{A4})$$

$$\mathcal{R}_{th_{22}} = \mathcal{R}_{th_{33}} = \frac{A_- + A_+ + 2 \left(\frac{B_-}{\alpha_-} + \frac{B_+}{\alpha_+} \right) \xi_c}{4(A_- + A_+)}, \quad (\text{A5})$$

$$\mathcal{R}_{th_{23}} = \mathcal{R}_{th_{32}} = \frac{-A_- + A_+ - \frac{2B_- \xi_c}{\alpha_-} + \frac{2B_+ \xi_c}{\alpha_+}}{4(A_- + A_+)}, \quad (\text{A6})$$

$$\mathcal{R}_{th_{43}} = \mathcal{R}_{th_{34}} = \frac{\frac{B_- (\xi_2 - \xi_1)}{2\alpha_-} + \frac{B_+ (\xi_1 + \xi_2)}{2\alpha_+}}{2(A_- + A_+)}, \quad (\text{A7})$$

with

$$\mathcal{Z} = 2(A_+ + A_-), \quad (\text{A8})$$

and

$$\alpha_{\pm} = \sqrt{4\xi_c^2 + (\xi_1 \pm \xi_2)^2},$$

$$A_{\pm} = \cosh\left(\frac{\alpha_{\pm}}{2T}\right),$$

$$B_{\pm} = \sinh\left(\frac{\alpha_{\pm}}{2T}\right).$$

Appendix B: Density matrix $\mathcal{R}_{\mathcal{X}}(t)$

The density matrix $\mathcal{R}_{\mathcal{X}}(t)$ (15) is given by

$$\mathcal{R}_{\mathcal{X}}(t) = \begin{pmatrix} \mathcal{R}_{\mathcal{X}11}(t) & \mathcal{R}_{\mathcal{X}12}(t) & \mathcal{R}_{\mathcal{X}13}(t) & \mathcal{R}_{\mathcal{X}14}(t) \\ \mathcal{R}_{\mathcal{X}21}(t) & \mathcal{R}_{\mathcal{X}22}(t) & \mathcal{R}_{\mathcal{X}23}(t) & \mathcal{R}_{\mathcal{X}24}(t) \\ \mathcal{R}_{\mathcal{X}31}(t) & \mathcal{R}_{\mathcal{X}32}(t) & \mathcal{R}_{\mathcal{X}33}(t) & \mathcal{R}_{\mathcal{X}34}(t) \\ \mathcal{R}_{\mathcal{X}41}(t) & \mathcal{R}_{\mathcal{X}42}(t) & \mathcal{R}_{\mathcal{X}43}(t) & \mathcal{R}_{\mathcal{X}44}(t) \end{pmatrix}, \quad (\text{B1})$$

where

$$\mathcal{R}_{\mathcal{X}11}(t) = \mathcal{R}_{\mathcal{X}44}(t) = -\frac{-2A_- \cos^2(2\tau) + A_+(\cos(4\tau) - 3) + \frac{4B_- \xi_c \cos^2(2\tau)}{\alpha_-} + \frac{2B_+(\xi_c \cos(4\tau) + \xi_c - 2(\xi_1 + \xi_2) \sin(2\tau))}{\alpha_+}}{8(A_- + A_+)}, \quad (\text{B2})$$

$$\mathcal{R}_{\mathcal{X}12}(t) = \mathcal{R}_{\mathcal{X}21}(t) = \frac{\cos(2\tau) \left(\sin(2\tau) \left(A_- - A_+ - \frac{2B_- \xi_c}{\alpha_-} - \frac{2B_+ \xi_c}{\alpha_+} \right) + \frac{B_- (\xi_2 - \xi_1)}{\alpha_-} + \frac{B_+ (\xi_1 + \xi_2)}{\alpha_+} \right)}{4(A_- + A_+)}, \quad (\text{B3})$$

$$\mathcal{R}_{\mathcal{X}13}(t) = \mathcal{R}_{\mathcal{X}31}(t) = \frac{\cos(2\tau) \left(\sin(2\tau) \left(A_- - A_+ - \frac{2B_- \xi_c}{\alpha_-} - \frac{2B_+ \xi_c}{\alpha_+} \right) + \frac{B_- (\xi_1 - \xi_2)}{\alpha_-} + \frac{B_+ (\xi_1 + \xi_2)}{\alpha_+} \right)}{4(A_- + A_+)}, \quad (\text{B4})$$

$$\mathcal{R}_{\mathcal{X}14}(t) = \mathcal{R}_{\mathcal{X}41}(t) = \frac{-2A_- \cos^2(2\tau) + 2A_+ \cos^2(2\tau) + \frac{4B_- \xi_c \cos^2(2\tau)}{\alpha_-} + \frac{2B_+ \xi_c (\cos(4\tau) - 3)}{\alpha_+}}{8(A_- + A_+)}, \quad (\text{B5})$$

$$\mathcal{R}_{\mathcal{X}22}(t) = \frac{\alpha_+ (-\alpha_- A_- (\cos(4\tau) - 3)) + \alpha_- A_+ (\cos(4\tau) + 1) + 4B_- (\xi_2 - \xi_1) \sin(2\tau) + 4(\alpha_- B_+ + \alpha_+ B_-) \xi_c \cos^2(2\tau)}{8\alpha_- \alpha_+ (A_- + A_+)}, \quad (\text{B6})$$

$$\mathcal{R}_{\mathcal{X}23}(t) = \mathcal{R}_{\mathcal{X}32}(t) = \frac{2 \cos^2(2\tau) \left(-A_- + A_+ + \frac{2B_+ \xi_c}{\alpha_+} \right) + \frac{2B_- \xi_c (\cos(4\tau) - 3)}{\alpha_-}}{8(A_- + A_+)}, \quad (\text{B7})$$

$$\mathcal{R}_{\mathcal{X}24}(t) = \mathcal{R}_{\mathcal{X}42}(t) = -\frac{\cos(2\tau) \left(\sin(2\tau) \left(A_- - A_+ - \frac{2B_- \xi_c}{\alpha_-} - \frac{2B_+ \xi_c}{\alpha_+} \right) + \frac{B_- (\xi_2 - \xi_1)}{\alpha_-} - \frac{B_+ (\xi_1 + \xi_2)}{\alpha_+} \right)}{4(A_- + A_+)}, \quad (\text{B8})$$

$$\mathcal{R}_{\mathcal{X}33}(t) = \frac{\alpha_+ (-\alpha_- A_- (\cos(4\tau) - 3)) + \alpha_- A_+ (\cos(4\tau) + 1) + 4B_- (\xi_1 - \xi_2) \sin(2\tau) + 4(\alpha_- B_+ + \alpha_+ B_-) \xi_c \cos^2(2\tau)}{8\alpha_- \alpha_+ (A_- + A_+)}, \quad (\text{B9})$$

$$\mathcal{R}_{\mathcal{X}34}(t) = \mathcal{R}_{\mathcal{X}43}(t) = -\frac{\cos(2\tau) \left(\sin(2\tau) \left(A_- - A_+ - \frac{2B_- \xi_c}{\alpha_-} - \frac{2B_+ \xi_c}{\alpha_+} \right) + \frac{B_- (\xi_1 - \xi_2)}{\alpha_-} - \frac{B_+ (\xi_1 + \xi_2)}{\alpha_+} \right)}{4(A_- + A_+)}. \quad (\text{B10})$$

Appendix C: Closed-form expressions for performance metrics of SQB

The assessment of the final state of the battery focuses on its ergotropy, which is quantified as the maximum work extractable in a cyclic unitary process. We calculate the ergotropy of our system based on X-gate charging as follows:

$$\mathcal{E} = \frac{\sin^2(\tau) \left[4\xi_c \left(\xi_c \cos(2\tau) \left(\frac{B_-}{\alpha_-} + \frac{B_+}{\alpha_+} \right) + \cos^2(\tau) (A_+ - A_-) \right) + \alpha_- B_- + \alpha_+ B_+ \right]}{A_- + A_+}. \quad (\text{C1})$$

On the other hand, the instantaneous power \mathcal{P} of the SQB is calculated as:

$$\mathcal{P} = \frac{\sin(2\tau) \left[\alpha_- \left\{ 4\alpha_+ (A_+ - A_-) \xi_c \cos(2\tau) + B_+ (8\xi_c^2 \cos(2\tau) + (\xi_1 + \xi_2)^2) \right\} + \alpha_+ B_- (8\xi_c^2 \cos(2\tau) + (\xi_1 - \xi_2)^2) \right]}{\alpha_- \alpha_+ (A_- + A_+)}. \quad (\text{C2})$$

Finally, the capacity \mathcal{K} of the SQB is computed as:

$$\mathcal{K} = \frac{2(A_- + A_+) \xi_c + \alpha_- B_- + \alpha_+ B_+}{2(A_- + A_+)}. \quad (\text{C3})$$

DISCLOSURES

The authors declare that they have no known competing financial interests.

DATA AVAILABILITY

No datasets were generated or analyzed during the current study.

[1] S. E. Crawford, R. A. Shugayev, H. P. Paudel, P. Lu, M. Syamlal, P. R. Ohodnicki, B. Chorpeneing, R. Gentry,

and Y. Duan, Quantum sensing for energy applications:

- Review and perspective, *Advanced Quantum Technologies* **4**, 2100049 (2021).
- [2] J.-P. Aumasson, The impact of quantum computing on cryptography, *Computer Fraud & Security* **2017**, 8 (2017).
 - [3] P. Radanliev, Artificial intelligence and quantum cryptography, *Journal of Analytical Science and Technology* **15**, 4 (2024).
 - [4] S. D. Bass and M. Doser, Quantum sensing for particle physics, *Nature Reviews Physics* , 1 (2024).
 - [5] C. L. Degen, F. Reinhard, and P. Cappellaro, Quantum sensing, *Reviews of modern physics* **89**, 035002 (2017).
 - [6] F. Campaioli, S. Gherardini, J. Q. Quach, M. Polini, and G. M. Andolina, Colloquium: quantum batteries, *Reviews of Modern Physics* **96**, 031001 (2024).
 - [7] J. Q. Quach, G. Cerullo, and T. Virgili, Quantum batteries: The future of energy storage?, *Joule* **7**, 2195 (2023).
 - [8] J. Quach, T. Virgili, G. Cerullo, K. McGhee, L. Ganzer, and D. Lidzey, Organic quantum batteries, in *International Conference on Ultrafast Phenomena* (Optica Publishing Group, 2020) pp. Tu4A–1.
 - [9] R. Alicki and M. Fannes, Entanglement boost for extractable work from ensembles of quantum batteries, *Physical Review E* **87**, 042123 (2013).
 - [10] A. Clerk, K. Lehnert, P. Bertet, J. Petta, and Y. Nakamura, Hybrid quantum systems with circuit quantum electrodynamics, *Nature Physics* **16**, 257 (2020).
 - [11] Z.-L. Xiang, S. Ashhab, J. You, and F. Nori, Hybrid quantum circuits: Superconducting circuits interacting with other quantum systems, *Reviews of Modern Physics* **85**, 623 (2013).
 - [12] M. Kjaergaard, M. E. Schwartz, J. Braumüller, P. Krantz, J. I.-J. Wang, S. Gustavsson, and W. D. Oliver, Superconducting qubits: Current state of play, *Annual Review of Condensed Matter Physics* **11**, 369 (2020).
 - [13] C.-K. Hu, J. Qiu, P. J. Souza, J. Yuan, Y. Zhou, L. Zhang, J. Chu, X. Pan, L. Hu, J. Li, *et al.*, Optimal charging of a superconducting quantum battery, *Quantum Science and Technology* **7**, 045018 (2022).
 - [14] R. Dell and D. A. J. Rand, *Understanding batteries*, Vol. 28 (Royal society of chemistry, 2001).
 - [15] J.-Y. Gyhm and U. R. Fischer, Beneficial and detrimental entanglement for quantum battery charging, *AVS Quantum Science* **6**, 012001 (2024).
 - [16] D. Ferraro, M. Campisi, G. M. Andolina, V. Pellegrini, and M. Polini, High-power collective charging of a solid-state quantum battery, *Physical review letters* **120**, 117702 (2018).
 - [17] F.-M. Yang and F.-Q. Dou, Resonator-qutrit quantum battery, *Physical Review A* **109**, 062432 (2024).
 - [18] B. Ahmadi, P. Mazurek, P. Horodecki, and S. Barzanjeh, Nonreciprocal quantum batteries, *Physical Review Letters* **132**, 210402 (2024).
 - [19] F. Pobell, *Matter and methods at low temperatures*, Vol. 2 (Springer, 2007).
 - [20] M. Pechal and A. H. Safavi-Naeini, Millimeter-wave interconnects for microwave-frequency quantum machines, *Physical Review A* **96**, 042305 (2017).
 - [21] P. Magnard, S. Storz, P. Kurpiers, J. Schär, F. Marxer, J. Lütolf, T. Walter, J.-C. Besse, M. Gabureac, K. Reuer, *et al.*, Microwave quantum link between superconducting circuits housed in spatially separated cryogenic systems, *Physical Review Letters* **125**, 260502 (2020).
 - [22] C.-H. Liu, A. Ballard, D. Olaya, D. R. Schmidt, J. Biesecker, T. Lucas, J. Ullom, S. Patel, O. Rafferty, A. Opremcak, *et al.*, Single flux quantum-based digital control of superconducting qubits in a multichip module, *PRX Quantum* **4**, 030310 (2023).
 - [23] S. Krinner, S. Storz, P. Kurpiers, P. Magnard, J. Heinsoo, R. Keller, J. Luetolf, C. Eichler, and A. Wallraff, Engineering cryogenic setups for 100-qubit scale superconducting circuit systems, *EPJ Quantum Technology* **6**, 2 (2019).
 - [24] Y. Wu, W.-S. Bao, S. Cao, F. Chen, M.-C. Chen, X. Chen, T.-H. Chung, H. Deng, Y. Du, D. Fan, *et al.*, Strong quantum computational advantage using a superconducting quantum processor, *Physical review letters* **127**, 180501 (2021).
 - [25] F. Kamin, F. Tabesh, S. Salimi, and A. C. Santos, Entanglement, coherence, and charging process of quantum batteries, *Physical Review E* **102**, 052109 (2020).
 - [26] H.-L. Shi, S. Ding, Q.-K. Wan, X.-H. Wang, and W.-L. Yang, Entanglement, coherence, and extractable work in quantum batteries, *Physical Review Letters* **129**, 130602 (2022).
 - [27] G. M. Andolina, D. Farina, A. Mari, V. Pellegrini, V. Giovannetti, and M. Polini, Charger-mediated energy transfer in exactly solvable models for quantum batteries, *Physical Review B* **98**, 205423 (2018).
 - [28] D. Rossini, G. M. Andolina, and M. Polini, Many-body localized quantum batteries, *Physical Review B* **100**, 115142 (2019).
 - [29] Y. Yao and X. Shao, Optimal charging of open spin-chain quantum batteries via homodyne-based feedback control, *Physical Review E* **106**, 014138 (2022).
 - [30] F.-Q. Dou, H. Zhou, and J.-A. Sun, Cavity heisenberg-spin-chain quantum battery, *Physical Review A* **106**, 032212 (2022).
 - [31] B. Mojaveri, R. Jafarzadeh Bahrbeig, and M. Fasihi, Extracting ergotropy from nonequilibrium steady states of an xxz spin-chain quantum battery, *Physical Review A* **109**, 042619 (2024).
 - [32] A. Ali, S. Al-Kuwari, M. I. Hussain, T. Byrnes, M. Rahim, J. Q. Quach, M. Ghomejad, and S. Haddadi, Ergotropy and capacity optimization in heisenberg spin-chain quantum batteries, *Physical Review A* **110**, 052404 (2024).
 - [33] M. Hadipour, S. Haseli, D. Wang, and S. Haddadi, Proposed scheme for a cavity-based quantum battery, *Advanced Quantum Technologies* **7**, 2400115 (2024).
 - [34] M. Shaw, J. F. Schneiderman, J. Bueno, B. Palmer, P. Delsing, and P. Echternach, Characterization of an entangled system of two superconducting qubits using a multiplexed capacitance measurement, *Physical Review B—Condensed Matter and Materials Physics* **79**, 014516 (2009).
 - [35] G. Paraoanu, Microwave-induced coupling of superconducting qubits, *Physical Review B—Condensed Matter and Materials Physics* **74**, 140504 (2006).
 - [36] J. Li, K. Chalapat, and G.-S. Paraoanu, Entanglement of superconducting qubits via microwave fields: Classical and quantum regimes, *Physical Review B—Condensed Matter and Materials Physics* **78**, 064503 (2008).
 - [37] L.-J. Tian, L.-G. Qin, and H.-B. Zhang, Entanglement of two-superconducting-qubit system coupled with a fixed capacitor, *Chinese Physics Letters* **28**, 050308 (2011).

- [38] A. E. Allahverdyan, R. Balian, and T. M. Nieuwenhuizen, Maximal work extraction from finite quantum systems, *Europhysics Letters* **67**, 565 (2004).
- [39] A. Lenard, Thermodynamical proof of the gibbs formula for elementary quantum systems, *Journal of Statistical Physics* **19**, 575 (1978).
- [40] W. Pusz and S. L. Woronowicz, Passive states and kms states for general quantum systems, *Communications in Mathematical Physics* **58**, 273 (1978).
- [41] R. Salvia and V. Giovannetti, On the distribution of the mean energy in the unitary orbit of quantum states, *Quantum* **5**, 514 (2021).
- [42] S. Ghosh, T. Chanda, A. Sen, *et al.*, Enhancement in the performance of a quantum battery by ordered and disordered interactions, *Physical Review A* **101**, 032115 (2020).
- [43] F. C. Binder, S. Vinjanampathy, K. Modi, and J. Goold, Quantacell: powerful charging of quantum batteries, *New Journal of Physics* **17**, 075015 (2015).
- [44] X. Yang, Y.-H. Yang, M. Alimuddin, R. Salvia, S.-M. Fei, L.-M. Zhao, S. Nimmrichter, and M.-X. Luo, Battery capacity of energy-storing quantum systems, *Physical Review Letters* **131**, 030402 (2023).
- [45] T. Baumgratz, M. Cramer, and M. B. Plenio, Quantifying coherence, *Physical Review Letters* **113**, 140401 (2014).